

Power-Law Scaling in the Classification Performance of Small-Scale Spiking Neural Networks

Zhengdi Zhang¹, Cong Han¹, Wenjun Xia^{1,*}

¹School of Mathematical Sciences, Jiangsu University.

*Corresponding author: vujqnwork@outlook.com.

Abstract

This paper investigates the classification capability of small-scale spiking neural networks based on the Leaky Integrate-and-Fire (LIF) neuron model. We analyze the relationship between classification accuracy and three factors: the number of neurons, the number of stimulus nodes, and the number of classification categories. Notably, we employ a large language model (LLM) to assist in discovering the underlying functional relationships among these variables, and compare its performance against traditional methods such as linear and polynomial fitting. Experimental results show that classification accuracy follows a power-law scaling primarily with the number of categories, while the effects of neuron count and stimulus nodes are relatively minor. A key advantage of the LLM-based approach is its ability to propose plausible functional forms beyond pre-defined equation templates, often leading to more concise or accurate mathematical descriptions of the observed scaling laws. This finding has important implications for understanding efficient computation in biological neural systems and for pioneering new paradigms in AI-aided scientific discovery.

Keywords: spiking neural networks, Leaky Integrate-and-Fire (LIF) neuron, AI-aided discovery, power law, function discovery, computational neuroscience

1 Introduction

As a cornerstone of computational neuroscience and neuromorphic engineering, spiking neural networks (SNNs) offer a biologically plausible framework for understanding information processing in the brain [3]. Among various neuron models, the Leaky

Integrate-and-Fire (LIF) model strikes an effective balance between biological realism and computational tractability, making it a widely adopted building block for studying network-level dynamics and computation [1, 2]. A long-standing question in the field concerns the fundamental relationship between the structural parameters of a neural network and its functional capacity, particularly in resource-constrained regimes reminiscent of biological systems. Prior investigations have often focused on isolated factors: some studies have examined how classification performance scales with the number of neurons, typically observing diminishing returns [5], while others have analyzed the impact of input dimensionality or task complexity on network accuracy. However, a systematic exploration that concurrently varies multiple key parameters—network size (neuron count), input dimensionality (stimulus node number), and task complexity (classification category number)—in LIF-based SNNs remains limited. Understanding their combined and relative influence is crucial for revealing efficiency principles in neural computation, especially in the small-scale regimes that may reflect fundamental computational units in biological circuits [4].

Recent advances in artificial intelligence have opened new avenues for accelerating scientific discovery. In particular, large language models (LLMs) have demonstrated emergent capabilities in reasoning, pattern recognition, and even proposing scientific hypotheses or functional relationships from complex datasets [6]. This aligns with a growing paradigm of "human-AI collaboration" in research, where AI assists in uncovering patterns or formulating models that might be non-intuitive or labor-intensive to derive using traditional analytical methods alone [7]. Such collaborative approaches have shown promise in fields ranging from material science to mathematical discovery [8].

In this work, we bridge these two strands of inquiry. We systematically investigate the classification capability of small-scale LIF spiking neural networks by conducting a multi-dimensional parameter sweep over neuron count, stimulus node number, and category number. Beyond employing conventional fitting techniques (e.g., linear and polynomial regression), we leverage a large language model as a collaborative tool to aid in discovering and interpreting the underlying functional relationships that govern network performance. Our study aims to: 1) quantify the scaling laws between classification accuracy and the three core parameters, drawing inspiration from scaling law research in artificial neural networks [9], 2) identify which factor exerts the dominant influence on performance in this constrained setting, and 3) demonstrate how AI-assisted analysis can complement traditional methods to uncover concise and interpretable mathematical descriptions of complex phenomena in computational neuroscience [10]. The findings not only elucidate fundamental constraints in spiking network performance but also contribute to the emerging methodology of human-AI collaborative scientific exploration.

2 Methods

2.1 Computational Model of Spiking Neuronal Networks

We constructed spiking neural network models based on the Leaky Integrate-and-Fire (LIF) neuron model. The dynamics of each neuron is governed by the following differential equation:

$$\tau_m \frac{dV}{dt} = -(V - E_L) + \frac{I_{\text{noise}} + I_{\text{syn}}}{g_L} + V_{\text{stim}} \quad (1)$$

where τ_m is the membrane time constant, V is the membrane potential, E_L is the resting (leakage reversal) potential, g_L is the leakage conductance, V_{stim} represents the external stimulus voltage, I_{noise} models intrinsic physiological variability, and I_{syn} is the total synaptic current received from other neurons. When V reaches the threshold V_{th} , a spike is generated, after which V is reset to V_{reset} and held during a refractory period τ_{ref} .

2.1.1 Synaptic Current Model

The total synaptic current I_{syn} is the sum of exponentially decaying excitatory ($I_{\text{syn,E}}$) and inhibitory ($I_{\text{syn,I}}$) currents:

$$\frac{dI_{\text{syn,E}}}{dt} = -\frac{I_{\text{syn,E}}}{\tau_{\text{syn,E}}} + \sum_{\text{exc. spikes}} \delta(t - t_{\text{spike}}) \cdot a_{\text{ex}} \quad (2)$$

$$\frac{dI_{\text{syn,I}}}{dt} = -\frac{I_{\text{syn,I}}}{\tau_{\text{syn,I}}} + \sum_{\text{inh. spikes}} \delta(t - t_{\text{spike}}) \cdot a_{\text{in}} \quad (3)$$

where a_{ex} and a_{in} are the excitatory and inhibitory synaptic current increments, respectively, $\tau_{\text{syn,E}}$ and $\tau_{\text{syn,I}}$ are the excitatory and inhibitory synaptic time constants, and $\delta(t)$ is the Dirac delta function.

2.1.2 Distance-Dependent Connection Probability and Synaptic Weight

Structural connectivity between neurons was established probabilistically based on their Euclidean distance. The probability p_{ij} of a directed connection from neuron i to neuron j follows a Gaussian decay, inspired by the model in [4]:

$$p_{ij} = p_{\text{max}} \cdot \exp \left(-\frac{\|\mathbf{x}_i - \mathbf{x}_j\|^2}{2\sigma_c^2} \right) \quad (4)$$

where p_{max} is the maximum connection probability, σ_c is the spatial standard deviation (controlling the spatial extent of connectivity), and $\mathbf{x}_i, \mathbf{x}_j$ are the positions of the pre- and post-synaptic neurons, respectively.

Synaptic Weight: Upon the establishment of a connection, the strength (weight) w_{ij} of the synapse from neuron i to neuron j is also modulated by distance, following

a Gaussian decay as defined in [4]:

$$w_{ij} = c \cdot \frac{1}{\sqrt{2\pi\sigma_w^2}} \cdot \exp\left(-\frac{\|\mathbf{x}_i - \mathbf{x}_j\|^2}{2\sigma_w^2}\right) \quad (5)$$

where c is a scaling factor ($c = \sigma_c \times 32$, with $\sigma_c = 1000$), and σ_w is the spatial standard deviation governing the weight distribution (typically, $\sigma_w = \sigma_c$). This ensures that physically closer neuron pairs tend to form stronger synaptic connections. Neurons were classified as excitatory (80%) or inhibitory (20%) and randomly distributed within the network space.

2.2 Stimulus Input Implementation

The stimulus input V_{stim} represents external voltage pulses delivered to the network. This input is uniquely defined by a programmable binary matrix $\mathbf{S} \in \{0, 1\}^{N_{\text{stim}} \times m}$, where N_{stim} denotes the total number of neurons in the network that receive external stimulation (i.e., the number of stimulus nodes), and m denotes the total number of defined time points within one stimulus cycle.

Matrix Structure:

- **Row Dimension:** Each row i ($1 \leq i \leq N_{\text{stim}}$) of the matrix corresponds to a specific stimulus node (i.e., a neuron receiving external input). The row vector $\mathbf{S}(i, :)$ defines the temporal sequence of pulses that this neuron will receive throughout the stimulus cycle.
- **Column Dimension:** Each column k ($1 \leq k \leq m$) corresponds to a specific stimulus time point. The column index k maps to an absolute time of $t_k = 200 \times (k - 1)$ milliseconds (ms). Thus, the time points are uniformly distributed along the time axis with an interval of 200 ms, covering a total duration of $200 \times (m - 1)$ ms.

Stimulus Encoding Rule: A rectangular voltage pulse with an amplitude of 500 mV is delivered to neuron i at the absolute time t_k ms if and only if the matrix element $\mathbf{S}(i, k) = 1$. The pulse lasts for 0.5 ms. If $\mathbf{S}(i, k) = 0$, no stimulus is applied at the corresponding time point t_k .

$$V_{\text{stim},j}(t) = \begin{cases} 500 \text{ mV} & \text{if } \exists k \in \{1, 2, \dots, m\} \text{ such that } \mathbf{S}(j, k) = 1 \text{ and } t \in [t_k, t_k + 0.5] \\ 0 \text{ mV} & \text{otherwise} \end{cases} \quad (6)$$

where $t_k = 200 \times (k - 1)$ ms.

2.3 Stimulus Matrix Generation and Classification Design

The stimulus matrices for each category were procedurally generated to ensure distinct yet controlled patterns for classification. For a given number of stimulus nodes (S), the binary matrix \mathbf{S}_c for a specific category c was generated as follows:

1. **Position Framing:** A distinct, contiguous block of positions (rows and time columns) within the $S \times m$ matrix was allocated for category c . This block served as the primary encoding region for that category.
2. **Sparsity Control:** Within this allocated block, a fixed percentage of elements (within a predefined range) were randomly set to '1', with the rest being '0'. The specific percentage was chosen consistently across categories to maintain comparable overall input strength.
3. **Instance Variability:** To capture pattern variation within a single category and provide robust training data, 10 distinct matrix instances were generated for each category c by repeating the random '1' assignment within its defined block and sparsity constraint. These 10 instances constituted the samples for that category.

The set of categories for an experiment was generated sequentially. The stimulus matrices for a 2-class problem ($C = 2$) were generated first, defining two distinct spatial-temporal blocks. To create a 3-class problem ($C = 3$), a new third category was generated by defining a new, distinct block and populating it with '1's according to the same sparsity rule, while retaining the original two categories unchanged. This process was repeated iteratively to extend to $C = 4, 5, \dots, 30$ classes, ensuring that the class structure was cumulative and directly comparable across different values of C .

Using this method, we generated a comprehensive stimulus set that traversed all combinations of:

- Stimulus nodes: $S = 1, 2, 3$
- Classification categories: $C = 2, 3, 4, \dots, 30$

This stimulation protocol provides a flexible and scalable encoding framework. By adjusting the scale of the matrix \mathbf{S} (i.e., N_{stim} and m) and its internal binary patterns, we can systematically control the complexity and distinctiveness of the input signals. This allows us to investigate the influence of network size (N), input dimensionality (N_{stim}), and task complexity (number of categories C , corresponding to the number of unique \mathbf{S}_c matrices) on the network's classification performance.

2.4 Network Architecture and Parameters

The fundamental network architecture maintained a physiological balance with 80% excitatory and 20% inhibitory neurons, consistent with cortical network organization. Network density was maintained at approximately 6000 cells/mm² across all network sizes. Each simulation comprised a 10-second stabilization period followed by 4 seconds of recording (4000 ms), with integration time steps of 0.1 ms. All results are based on 100 independent trials per parameter configuration to ensure statistical robustness.

We systematically varied three key parameters across simulation ensembles with the following constraints:

- **Number of neurons (N):** 1, 2, 3
- **Number of stimulus nodes (S):** 1, 2, 3, with the constraint $S \leq N$
- **Number of classification categories (C):** 2, 3, 4, 5, ..., 30 (i.e., all integers from 2 to 30)

For each parameter combination (N, S, C) satisfying $S \leq N$, we designed 5 distinct simulation groups. In each group, a unique set of stimulus matrices $\{\mathbf{S}_c\}$ was generated for each category $c \in \{1, 2, \dots, C\}$ based on the given S and C . While the stimulus matrices differed across groups, they were generated under the same parameter conditions (i.e., same S and C), ensuring that the results capture the variability due to different input patterns and providing statistical robustness.

This full-factorial design with multiple stimulus realizations allowed us to systematically explore the independent and interactive effects of network scale, input dimensionality, and task complexity on classification performance, while accounting for the variability in input encoding.

2.5 Classification Task and Performance Evaluation

Following the generation of stimulus matrices and network simulation, the resulting spiking activity was processed for classification analysis. For each stimulus presentation, the network's response was captured as a binary spike matrix $\mathbf{R} \in \{0, 1\}^{N \times T'}$, where N is the number of neurons and T' is the number of recording time steps. An element $\mathbf{R}(i, \tau) = 1$ indicates that neuron i fired a spike at time step τ .

To extract compact and informative features, we performed **coordinate compression** on each output spike matrix \mathbf{R} . This process involved identifying all matrix coordinates (i, τ) where $\mathbf{R}(i, \tau) = 1$, representing the spatial (neuron index) and temporal (time bin) locations of each spike event. These coordinates were then aggregated and binned across the population and over time to form a fixed-dimensional feature vector for each trial.

Classification was performed using **linear logistic regression** (multinomial logistic regression for multi-class problems). For a C -class problem, the model computes a linear score for each class c based on the feature vector \mathbf{x} :

$$z_c = \mathbf{w}_c^T \mathbf{x} + b_c,$$

where \mathbf{w}_c is the weight vector and b_c is the bias term for class c . The probability that a sample belongs to class c is given by the softmax function:

$$P(y = c \mid \mathbf{x}) = \frac{e^{z_c}}{\sum_{j=1}^C e^{z_j}}.$$

The model was trained by minimizing a cross-entropy loss function with L2 regularization to prevent overfitting.

For each parameter configuration (N, S, C) , the dataset was randomly split into training (80% of trials) and testing (20% of trials) sets. The linear logistic regression classifier was trained on the training set and evaluated on the held-out test set. To account for variability in the data split, this training and testing procedure was repeated 10 times with different random partitions. The classification accuracy for each run was computed as the percentage of correctly classified test samples, and the **average accuracy across these 10 runs** was taken as the final performance metric

for that configuration. This metric served as our primary measure of the network's classification capability.

This evaluation protocol allowed us to systematically quantify how classification accuracy scales with the number of neurons (N), stimulus nodes (S), and categories (C), while controlling for stochasticity in both stimulus generation and network dynamics.

2.6 AI-Assisted Discovery of Functional Relationships

Prior to formulating the final additive power-law model (Equation 7), we explored multiple traditional and machine learning approaches to characterize the relationship between classification accuracy and the three independent variables (C, S, N). This exploration process was significantly accelerated and enhanced by collaboration with a large language model (LLM), specifically leveraging its capability to propose, evaluate, and refine mathematical hypotheses.

Initial Exploration with Traditional Methods: We first employed several conventional regression techniques (see model comparison in Figure 1):

- **Linear Regression:** Simple linear models $f(C, S, N) = \beta_0 + \beta_1 C + \beta_2 S + \beta_3 N$ yielded poor fit ($R^2 = 0.6696$), failing to capture the nonlinear relationship.
- **Polynomial Regression:** Second-order polynomial models with interaction terms achieved moderate performance ($R^2 = 0.6788$) but lacked interpretability, with coefficients having no clear physical meaning (Equation: $f(C, S, N) = 0.9721 - 0.0107C - 0.0541S - 0.0510N + 0.0017C \cdot S - 0.0009C \cdot N + 0.0134S \cdot N$).
- **Symbolic Regression using a Genetic Algorithm (GA):** A GA-based symbolic regression was employed to search for an optimal mathematical expression. However, this method is inherently constrained by a predefined set of mathematical symbols and operators, limiting its flexibility in discovering diverse functional forms. The discovered expression achieved moderate accuracy ($R^2 = 0.7372$) but was complex and unintuitive: $f(C, S, N) = \sqrt{\sqrt{\sqrt{(C \cdot N)^{-1}}}}$. While suggesting a potential power-law relationship between C and accuracy, the specific nested radical structure offered limited mechanistic insight and was difficult to interpret meaningfully within the context of neural network dynamics.
- **Random Forest (RF):** A non-parametric RF model achieved exceptional predictive accuracy ($R^2 = 0.9839$, RMSE = 0.0139) and robustly identified the number of categories (C) as the dominant feature, accounting for 83.78% of the explained variance (feature importance analysis shown in Figure 2). However, as a black-box model, it provided no explicit functional form. Notably, the feature importance results from RF strongly aligned with the insights later refined by the LLM, both highlighting the overwhelming influence of C on the functional relationship.

LLM-Guided Hypothesis Generation and Refinement: The outstanding performance of the Random Forest model confirmed the dominant role of C but left the exact functional relationship opaque. Similarly, while symbolic regression (GA) indicated a power-law scaling, its output was not interpretable. To bridge this gap, we engaged in an interactive, iterative dialogue with a state-of-the-art LLM, which

effectively synthesized the strengths of both data-driven approaches: the power-law insight from symbolic regression and the clear feature dominance from Random Forest. The process involved:

1. **Problem Framing:** Presenting the RF feature importance results (Figure 2) and the core scientific question: "What is a parsimonious, interpretable mathematical function that describes how classification accuracy scales with task complexity (C), given minor corrections from network parameters (S, N)?"
2. **Hypothesis Generation:** Building on the power-law hint from symbolic regression, the LLM proposed several candidate function families based on common scaling laws in complex systems: exponential decay ($e^{-\lambda C}$), logarithmic decay ($a - b \ln C$), and power-law decay (aC^b).
3. **Interactive Refinement:** We iteratively tested these proposals on our dataset. The LLM assisted in formulating the specific additive structure $f(C, S, N) = g(C) + h(S) + k(N)$ based on the RF insight that C was dominant while S and N had smaller, approximately linear effects. The LLM also suggested testing both multiplicative and additive combinations of the power-law term with the linear terms.
4. **Model Selection:** Quantitative comparison (Figure 1) showed that while the Random Forest achieved the highest predictive accuracy ($R^2 = 0.9839$), it lacked interpretability. Among interpretable models, the additive power-law model (Equation 7) offered the best balance between performance and interpretability, providing clear physical insights into the scaling relationship while maintaining reasonable predictive accuracy. This final model can be viewed as a synthesis: it incorporates the power-law scaling of C (as suggested by symbolic regression) within a simple, additive framework that respects the relative influence of variables as identified by Random Forest.

This collaborative, human-AI workflow allowed us to efficiently navigate a vast space of potential models. While data-driven methods like Random Forest achieved superior predictive performance and symbolic regression hinted at key scaling, the LLM-guided analytical approach integrated these insights to lead us to a physically interpretable scaling law that provides mechanistic understanding of the underlying phenomena—an insight that might have been obscured by purely data-driven black-box models.

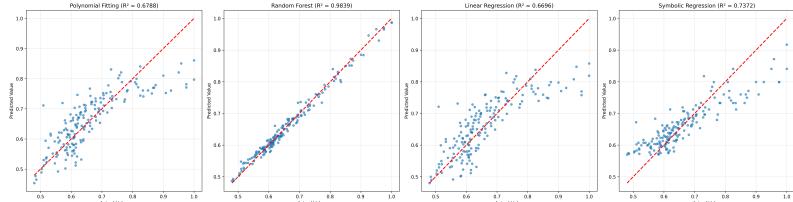


Fig. 1 Comparison of model predictions against actual values. The diagonal red line represents perfect prediction. All four models show varying degrees of accuracy, with Random Forest achieving near-perfect alignment.

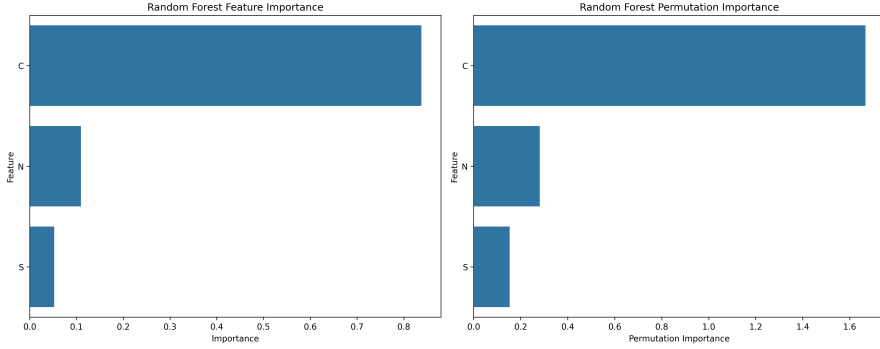


Fig. 2 Feature importance analysis for the Random Forest model. (Left) Standard feature importance shows C (number of categories) is the dominant predictor, accounting for 83.78% of the explained variance. (Right) Permutation importance confirms the robustness of this finding. This result is consistent with the LLM’s guidance, both emphasizing the critical role of C in determining the functional relationship.

2.7 Model Parameters

The complete set of model parameters is summarized in the following tables.

Table 1 Neuron Model Parameters

Parameter	Symbol	Value
Membrane time constant	τ_m	10 ms
Resting potential	V_{rest}	-70 mV
Threshold potential	V_{th}	-50 mV
Reset potential	V_{reset}	-70 mV
Refractory period	τ_{ref}	3 ms
Leakage conductance	g_L	10 nS
Noise current range	I_{noise}	$[0, 0.5]$ pA

3 Results

3.1 Power-Law Scaling Induced by Spiking Network Processing

Our central finding reveals that the power-law relationship between classification accuracy and task complexity emerges specifically from the processing of small-scale spiking neural networks, rather than being inherent to the stimulus patterns themselves. To establish this, we conducted a control experiment comparing direct stimulus classification with network-mediated classification.

Control experiment results: Direct application of linear logistic regression to the raw binary stimulus matrices \mathbf{S} (bypassing the network) yielded consistently high accuracy (> 0.85) across all category numbers $C = 2$ to 30. A power-law fit to this control data produced an exponent $b_{control} \approx -0.005$ with poor explanatory

Table 2 Synaptic and Input Parameters

Parameter	Symbol	Value
Excitatory synaptic weight	α_{EX}	10
Inhibitory synaptic weight	α_{IN}	20
Synaptic time constant	τ_{syn}	10 ms
Stimulus voltage amplitude	V_{stim}	500 mV
Stimulus pulse duration	T_{pulse}	0.5 ms
Inter-stimulus interval	T_{ISI}	200 ms
Excitatory synaptic time constant	$\tau_{\text{syn,E}}$	2 ms
Inhibitory synaptic time constant	$\tau_{\text{syn,I}}$	5 ms
Gaussian connection σ	σ_{conn}	1000 μm
Max connection probability	p_{MAX}	0.25

power ($R^2 < 0.1$), indicating no significant scaling relationship between accuracy and category number in the raw stimulus patterns.

Network experiment results: In contrast, classification based on the network’s spiking responses to identical stimuli showed a pronounced decay with increasing C , universally lower accuracy than the control, and followed a clear power-law relationship. This demonstrates that the power-law scaling is **imposed by the spiking neural network’s computational process**, not present in the input stimuli themselves. The transformation from highly separable stimulus patterns to dynamic spiking representations in resource-constrained networks introduces a fundamental bottleneck manifesting as a power-law trade-off.

3.2 Additive Power-Law Model for Network Classification Performance

To quantitatively characterize the network’s classification capability, we developed an ensemble additive power-law model incorporating three key variables: number of categories (C), stimulus nodes (S), and neurons (N). Based on data from five independent experimental runs (870 total samples), the model takes the form:

$$\text{Accuracy}(C, S, N) = p_1 \times C^{p_2} + p_3 \times S + p_4 \times N + p_5 \quad (7)$$

where C is the number of categories, S is the number of stimulus nodes, N is the number of neurons, and p_1 through p_5 are fitted parameters.

3.2.1 Model Parameters and Performance

The model was fitted to the combined dataset using nonlinear regression. The final parameter values and their interpretation are:

- $p_1 = 3.150233$: Scaling factor for the power-law term, representing baseline influence of category number
- $p_2 = -0.054043$: Exponent for parameter C . This negative value confirms power-law decay of accuracy with increasing categories in the network

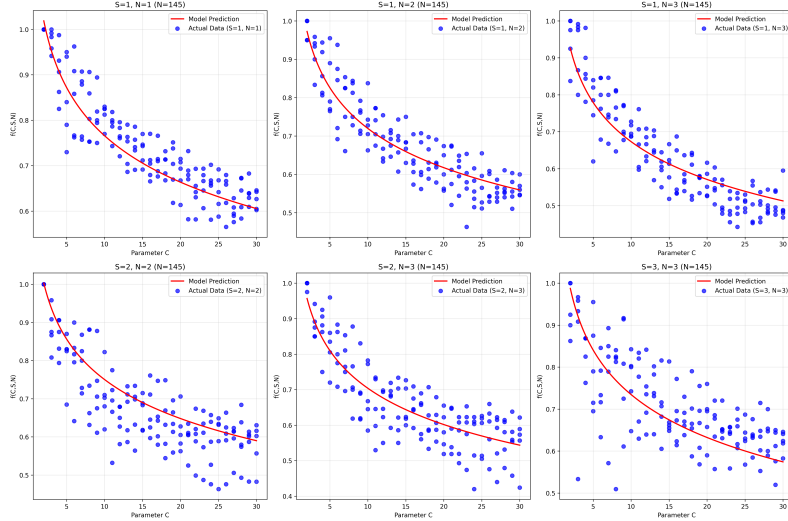


Fig. 3 Power-law fitting of classification accuracy as a function of the number of categories (C) under different combinations of stimulus nodes (S) and neurons (N). Each subplot shows the accuracy scaling for a specific (S, N) combination, demonstrating the consistent power-law relationship across all network configurations.

- $p_3 = 0.030683$: Linear coefficient for stimulus node count S , indicating small positive contribution from input dimensionality
- $p_4 = -0.046350$: Linear coefficient for neuron count N , showing slight negative trend possibly reflecting complexity in very small networks
- $p_5 = -2.000000$: Constant offset for baseline adjustment

The model demonstrates strong explanatory power with coefficient of determination $R^2 = 0.761$, mean absolute error (MAE) = 0.049, and root mean square error (RMSE) = 0.062.

3.2.2 Model Validation and Stability

Five-fold cross-validation confirmed model robustness: mean $R^2 = 0.756 \pm 0.039$ across folds. Parameter estimates remained stable:

- $p_1 : 3.150353 \pm 0.009$
- $p_2 : -0.054061 \pm 0.001$
- $p_3 : 0.030695 \pm 0.001$
- $p_4 : -0.046347 \pm 0.002$
- $p_5 : -1.999980 \pm 0.000$

Small standard deviations confirm parameter reliability and model generalizability.

Additional diagnostic analyses, including residual analysis and distribution comparisons, are provided in the Appendix for completeness.

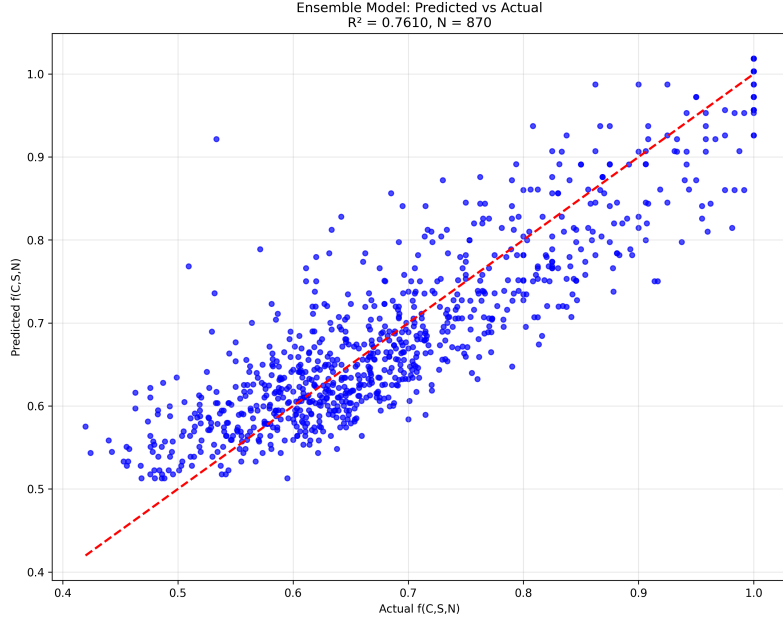


Fig. 4 Scatter plot of predicted versus actual classification accuracy for the ensemble model. Close alignment along the diagonal demonstrates good predictive accuracy across the full value range.

3.3 Control Experiment: Analysis of Stimulus Input Classification Without Neuronal Networks

We further analyzed the power-law relationships Accuracy = $a \times C^b$ for stimulus input classification data (direct classification on stimulus inputs without the involvement of neuronal networks), under fixed stimulus node counts S :

Table 3 Power-law fits of classification accuracy vs. C for fixed stimulus node counts (no neuronal networks involved)

Stimulus Nodes (S)	Data Points	a	b (Exponent)	R^2 (Quality)
1	145	1.017	-0.038	0.150 (Poor)
2	145	1.047	-0.030	0.234 (Poor)
3	145	1.011	-0.006	0.202 (Poor)

Table 3 shows negative exponents b across all S (confirming a decreasing trend of accuracy with increasing C), but extremely poor individual fits ($R^2 < 0.5$). Notably, these poor fits directly indicate that there is **no valid power-law distribution between stimulus inputs and the number of categories** in the absence of neuronal networks. Fitting quality classification: Excellent ($R^2 > 0.9$), Good (> 0.7), Fair (> 0.5), Poor (≤ 0.5).

The poor fitting performance underscores two key points: first, considering only C is insufficient to characterize the relationship; second, more importantly, the core conclusion that the power-law distribution does not hold for direct stimulus input classification without neuronal network participation. Additive terms for S and N in Equation 7 are originally necessary to explain variance from network architecture and resource limits, but this experiment further verifies that such power-law characteristics are even non-existent in the scenario without neuronal networks.

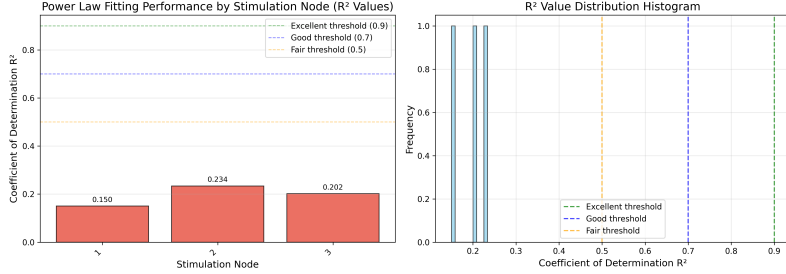


Fig. 5 Power-law fitting performance for stimulus input classification data under fixed stimulus node counts ($S = 1, 2, 3$) (no neuronal networks involved). Scatter plots show direct classification accuracy data, lines show individual power-law fits from Table 3. Wide point dispersion relative to fit lines visually confirms "Poor" R^2 ratings and the absence of valid power-law distribution.

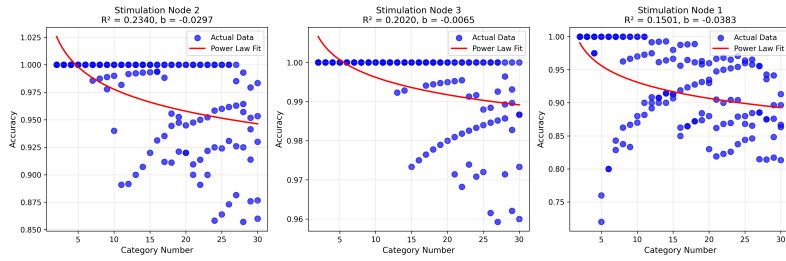


Fig. 6 Representative power-law fits for specific fixed parameter combinations (S, N) without neuronal network involvement. Visualizes the decaying trend of direct classification accuracy with C under specific constraints, with no observable power-law regularity.

3.4 Interpretation and Key Findings

The ensemble model and comparative analysis reveal important insights:

1. **Network-induced power-law scaling:** The power-law relationship between classification accuracy and task complexity is not inherent in stimuli but emerges from spiking network processing. Control experiment shows direct stimulus classification maintains high accuracy without significant decay, while network-mediated classification exhibits clear power-law decay.

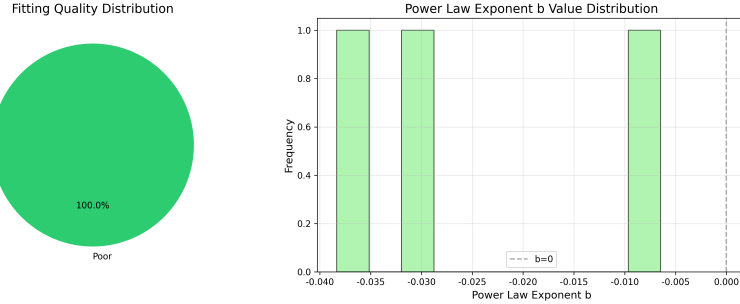


Fig. 7 Distribution of fitting quality for simple power-law models (Accuracy = $a \times C^b$) across stimulus input parameter combinations (no neuronal networks involved). Prevalence of "Poor" fits reinforces the core conclusion that there is no power-law distribution between stimulus inputs and the number of categories.

2. **Dominant power-law relationship with categories:** Primary determinant of network classification accuracy is number of categories C , following power-law decay. Exponent $p_2 = -0.054$ indicates gradual decrease as C increases, reflecting fundamental challenge of discriminating more classes with limited network resources.
3. **Minor linear network parameter effects:** Stimulus node count S and neuron count N show small linear contributions. Positive S coefficient suggests modest benefits from additional input channels; negative N coefficient may indicate complexity in very small networks (1-3 neurons).
4. **Predominance of task complexity:** Relative coefficient magnitudes confirm task complexity (categories) has substantially larger impact on classification performance than network size or input dimensionality in our experimental regime.

These results demonstrate that even in extremely small neural networks (1-3 neurons), classification accuracy follows predictable scaling laws induced by network processing, with task complexity being the dominant factor. The additive power-law model provides a quantitative framework for understanding network architecture and classification capability interplay in resource-constrained regimes.

4 Conclusion

This study has systematically investigated the classification capabilities of extremely small-scale spiking neural networks. Our central finding is that the classification accuracy of networks composed of only 1 to 3 neurons follows a precise and predictable scaling law, which is predominantly characterized by a power-law decay with the number of task categories. The empirically derived additive power-law model, $\text{Accuracy} = p_1 \times C^{p_2} + p_3 \times S + p_4 \times N + p_5$, successfully captures this relationship, with the negative exponent $p_2 = -0.054$ quantifying the rate of performance decline as task complexity increases.

Crucially, a dedicated control experiment demonstrated that this power-law scaling is not an inherent property of the stimulus patterns themselves—which remained highly separable under direct classification—but is a fundamental computational

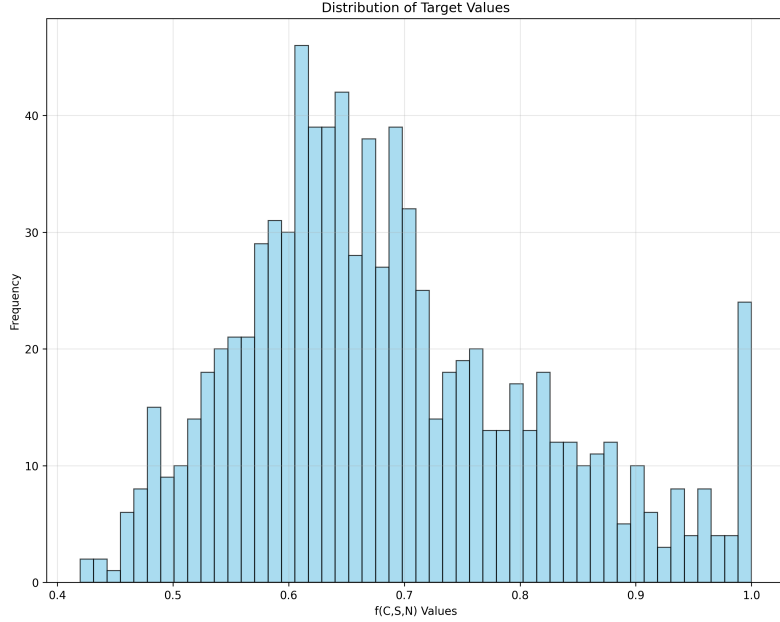


Fig. 8 Frequency distribution histogram of classification accuracy (represented by $f(C, S, N)$ values). The horizontal axis denotes the actual classification accuracy (i.e., $f(C, S, N)$ values), while the vertical axis indicates the frequency of occurrence for each accuracy value. The multimodal distribution feature presented in the figure intuitively reflects the variability in task difficulty across different (S, N, C) parameter combinations: each peak corresponds to a concentrated region of accuracy under specific parameter configurations, meaning some parameter combinations form task groups with similar difficulty, and their classification accuracies are relatively clustered.

bottleneck induced by the spiking neural network. This underscores that the transformation of information within a dynamic, resource-constrained spiking framework imposes intrinsic limits on performance, revealing a core trade-off between task complexity and computational capacity.

Methodologically, this work highlights the value of human-AI collaboration in scientific discovery. The path to this interpretable scaling law was significantly accelerated by leveraging a large language model as a hypothesis-generation partner. After traditional methods (linear/polynomial regression, genetic algorithms) failed to yield both accuracy and interpretability, and while a random forest model confirmed the dominant role of category number (C), the AI aided in efficiently exploring and refining candidate function families, leading to the concise and insightful power-law formulation.

Future Perspectives and Implications

The findings and methodology open several promising directions for future research and carry practical implications:

Extending Network Complexity: Future work should explore how this scaling law is modulated by richer biological details. This includes investigating the effects of varied

excitatory-inhibitory balances, structured inter-network connectivity (e.g., modular designs), and the inclusion of synaptic plasticity rules, all of which could alter the network’s dynamical regime and information-processing capacity.

Theoretical Underpinnings: While the power-law relationship is empirically robust, its theoretical origin invites deeper exploration. Deriving a similar scaling exponent from first principles—potentially from information-theoretic constraints or the statistical mechanics of neural dynamics—would provide a more fundamental understanding of why this specific functional form emerges.

Dissecting Minor Influences: The small but statistically significant linear effects of neuron count (N) and stimulus node count (S) warrant finer mechanistic study. Future analyses could examine how these parameters influence the network’s effective dimensionality, representational sparsity, or signal-propagation fidelity to explain their specific, albeit minor, roles.

Guidance for Neuromorphic Engineering: This scaling law provides a concrete, quantitative design principle for resource-efficient brain-inspired computing hardware. For a fixed neuromorphic core with a limited number of artificial neurons, the law predicts a hard performance boundary for classification tasks. This enables hardware designers to optimize resource allocation, implement intelligent task scheduling, or architect scalable multi-core systems where computational loads are distributed in accordance with predictable performance limits.

In summary, this research bridges microscopic neuron models with network-level computational principles, demonstrating that even the smallest neural ensembles adhere to rigorous scaling laws. By combining rigorous simulation with AI-aided discovery, we have established a framework for quantifying the efficiency of neural computation, offering valuable perspectives for both understanding biological neural systems and engineering the next generation of efficient, brain-inspired artificial intelligence.

Appendix A Supplementary Model Diagnostics

The following supplementary figures provide additional diagnostic information about the additive power-law model’s performance and residual characteristics.

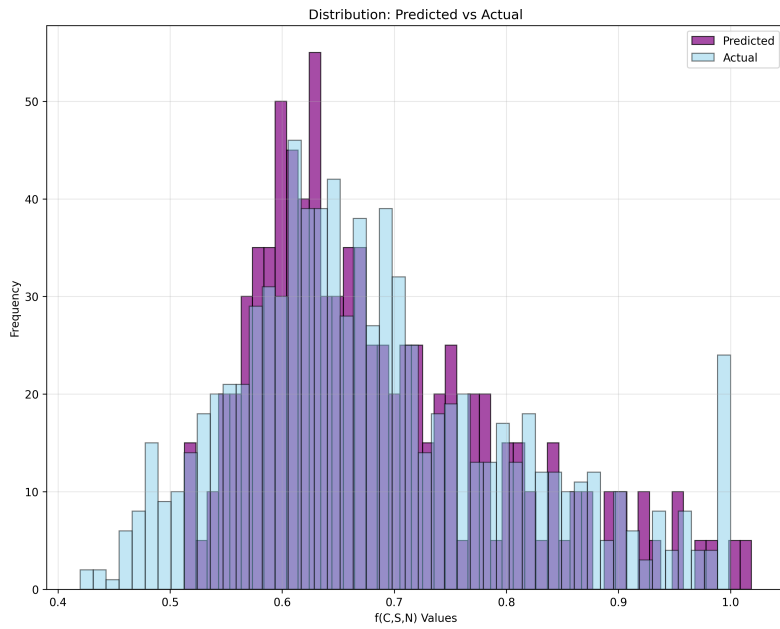


Fig. A1 Distribution comparison between predicted and actual accuracy values. Similar central tendencies and dispersion confirm the model captures the overall data structure.

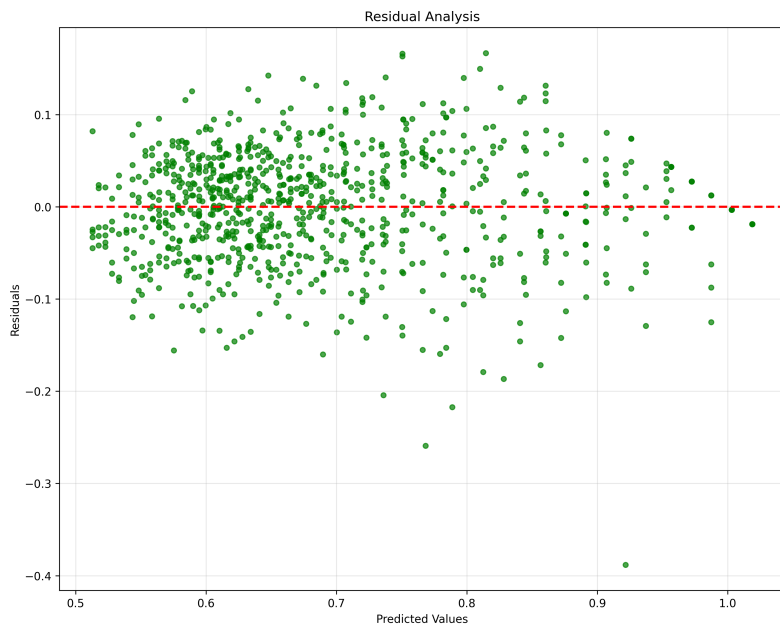


Fig. A2 Residual analysis showing distribution of prediction errors across accuracy values. Relatively uniform spread indicates good model fit without systematic biases.

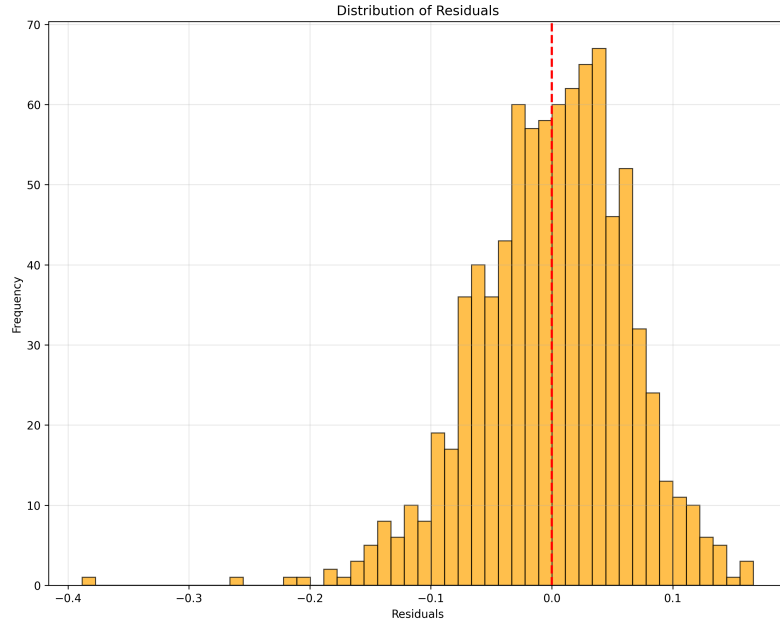


Fig. A3 Distribution of model residuals. Approximately normal distribution centered near zero confirms random, unbiased prediction errors.

References

- [1] Izhikevich, E. M. (2003). Simple model of spiking neurons. *IEEE Transactions on neural networks*, 14(6), 1569-1572.
- [2] Gerstner, W., Kistler, W. M., Naud, R., & Paninski, L. (2014). *Neuronal dynamics: From single neurons to networks and models of cognition*. Cambridge University Press.
- [3] Maass, W. (1997). Networks of spiking neurons: The third generation of neural network models. *Neural networks*, 10(9), 1659-1671.
- [4] Callegari, F., Brofiga, M., & Massobrio, P. (2023). Modeling the three-dimensional connectivity of in vitro cortical ensembles coupled to Micro-Electrode Arrays. *PLOS Computational Biology*, 19(2), e1010825.
- [5] Pfeiffer, M., & Pfeil, T. (2018). Deep learning with spiking neurons: Opportunities and challenges. *Frontiers in neuroscience*, 12, 774.
- [6] Bran, A. M., Cox, S., White, A. D., & Schwaller, P. (2024). Augmenting large language models with chemistry tools. *Nature Machine Intelligence*, 6(5), 525-535.

- [7] Guo, T., et al. (2024). Towards Large Language Models as Copilots for Theorem Proving in Lean. arXiv preprint arXiv:2406.04538.
- [8] Bubeck, S., et al. (2023). Sparks of artificial general intelligence: Early experiments with gpt-4. arXiv preprint arXiv:2303.12712.
- [9] Kaplan, J., et al. (2020). Scaling laws for neural language models. arXiv preprint arXiv:2001.08361.
- [10] Alabdulmohsin, I., et al. (2024). A Law of Scaling for Machine Learning. arXiv preprint arXiv:2406.06278.